

https://dspace.org/

Improved Adsorption and Photocatalytic Degradation of Methyl Orange by Onion-like Nanocarbon/TiO2 Nanocomposites

Ntuli, Themba D.; Sikeyi, Ludwe L.; Dziike, Faria; Coville, Neil J.; Nxumalo, Edward N. ...

2023-04
MDPI
https://hdl.handle.net/10539/50263
Ntuli, T.D.; Sikeyi, L.L.; Dziike, F.; Coville, N.J.; Nxumalo, E.N.; Maubane-Nkadimeng, M.S. Improved Adsorption and Photocatalytic Degradation of Methyl Orange by Onion-like Nanocarbon/ TiO2 Nanocomposites. Appl. Sci. 2023, 13, 5125. https://doi.org/ 10.3390 /app13085125

Downloaded from a DSpace repository. https://dspace.org/

applied sciences

MDPI

Article

Improved Adsorption and Photocatalytic Degradation of Methyl Orange by Onion-like Nanocarbon/TiO_2 Nanocomposites

Themba D. Ntuli [1,2], Ludwe L. Sikeyi [2], Faria Dziike [3], Neil J. Coville [1,2], Edward N. Nxumalo [4] and Manoko S. Maubane-Nkadimeng [1,2,5,*]

1 DSI-NRF Centre of Excellence in Strong Materials, School of Chemistry, University of the Witwatersrand, Private Bag 3, Johannesburg 2050, South Africa; 1888266@students.wits.ac.za (T.D.N.); neil.coville@wits.ac.za (N.J.C.)
2 The Molecular Sciences Institute, School of Chemistry, University of the Witwatersrand, Private Bag 3, Johannesburg 2050, South Africa; 2303563@students.wits.ac.za
3 Technology Transfer and Innovation Directorate, Steve Biko Campus, Durban University of Technology, Durban 4000, South Africa
4 Institute for Nanotechnology and Water Sustainability, College of Science, Engineering and Technology, University of South Africa, Private Bag X6, Florida 1709, South Africa
5 Microscopy and Microanalysis Unit, University of the Witwatersrand, Private Bag 3, Johannesburg 2050, South Africa
* Correspondence: manoko.maubane@wits.ac.za

Abstract: Waste cooking oil, a known environmental pollutant, has been used as a precursor for the synthesis of onion-like nanocarbons (OLNCs) using flame pyrolysis. The OLNCs were added to TiO_2 to form TiO_2/OLNC nanocomposites through hydrothermal treatment. The TiO_2/OLNCs ratio was varied by increasing the mass of the OLNCs (10, 20, 30, and 50 mg), while the mass of TiO_2 (100 mg) was kept constant at C to TiO_2 molar ratios of 1:2, 1:4, 1:6, and 1:10, respectively. The surface area of the photocatalysts increased with an increase in the mass of OLNCs. The nanocomposites were applied in the photocatalytic degradation of methyl orange. The photocatalysts showed a degradation efficiency trend of TC-10 > (99.9%) TC-20 > (90%) TC-30 > (81%) TC-50 > (70%) TiO_2 (44%) in 120 min. A similar trend was observed from the first-order kinetic rate data. The degradation efficiency of methyl orange was improved by adding 5% H_2O_2 (99.9%) in 30 min. The OLNCs were responsible for increased photocatalytic activity due to a high adsorption efficiency compared to pure TiO_2. The OLNCs acted as an electron acceptor, while the TiO_2 acted as an electron donor. The enhanced catalytic behavior was achieved by hindering the recombination of e^-/h^+ in the composite and increasing the adsorption capability of TiO_2.

Keywords: nanocomposites; solar irradiation; photodegradation; anatase; methyl orange; onion-like nanocarbons

check for updates

Citation: Ntuli, T.D.; Sikeyi, L.L.; Dziike, F.; Coville, N.J.; Nxumalo, E.N.; Maubane-Nkadimeng, M.S. Improved Adsorption and Photocatalytic Degradation of Methyl Orange by Onion-like Nanocarbon/TiO_2 Nanocomposites. *Appl. Sci.* **2023**, *13*, 5125. https://doi.org/10.3390/app13085125

Academic Editors: Ntaote David Shooto and Fanyana M. Mtunzi

Received: 8 March 2023
Revised: 13 April 2023
Accepted: 18 April 2023
Published: 20 April 2023

Copyright: © 2023 by the authors. Licensee MDPI, Basel, Switzerland. This article is an open access article distributed under the terms and conditions of the Creative Commons Attribution (CC BY) license (https://creativecommons.org/licenses/by/4.0/).

1. Introduction

Recent innovations and technological developments have given rise to interest in advanced oxidation processes (AOPs), which are an effective application in solving serious water pollution problems. Among the many AOPs, the photo-Fenton process has become an attractive alternative method for removing pollutants from water bodies due to its environmental friendliness, suitable price, and wide range of applications [1]. Similarly, semiconducting materials have been used in electro-photocatalysis technology, and have attracted extensive attention due to their low price and lack of secondary pollution. A typical semiconductor catalyst material, TiO_2, has been widely studied due to its high efficiency, non-toxicity, and low cost. However, the wide band gap (3.2 eV) of TiO_2 limits its utilization of visible light.

Thus, a semiconductor material with high visible-light utilization is an important parameter. The ternary oxyhalide semiconductor BiOBr is a new type of photocatalyst with

a lower bandgap (2.7 eV), high stability, and special layered structure, and is widely used in sensors, catalysts, and optics. In a single tetragonal BiOBr cell, layered [Bi_2O_2] and bromine atoms are alternately arranged [2].

Surface chemical materials with a unique mechanism of contaminant removal have been explored as an alternative. Grafting magnetic nanoparticles onto amino functional groups yields amino-functionalized magnetic nanoparticles. The material shows more efficient performance than bare magnetic nanoparticles in water treatment applications. Their magnetic nature is crucial for cost-effective and greener pollutant removal from water, since they are magnetically separated and can be reused without a major change in structure and efficiency [3].

However, the development of Fenton mimicking heterogeneous processes still dominates interest in environmental remediation research. Ferrocene is a highly stable, non-toxic, organometallic compound with high catalytic potential due to its electron donor−acceptor conjugated structure, which serves as a redox switch. The technology uses a supported ionic liquid phase (SILP) catalyst that involves the grafting of ionic liquid-like units onto a porous material with a high surface area. A highly striking strategy is offered by these advanced materials to overcome the impact of ionic liquids, and it opens up a new perspective for powerful green tools and recognizes the goal of sustainable chemical processes [4].

Among the other attempts to improve the performance of the photocatalyst are doping with anionic/cationic species, which has been widely explored [5].

There are two prevailing (complementary) schools of thought on how to improve the use of semiconducting materials as photocatalysts: (i) harvesting visible light, and (ii) decreasing the rate at which the generated hole (h^+) and electrons (e^-) recombine [6]. Carbon materials can potentially satisfy both requirements. Carbon materials such as carbon spheres [7], carbon fibers, carbon nanotubes [8], and activated carbon [9] are attractive as an additive to semiconducting metal oxides that form photocatalytic nanocomposites [10].

Carbon-rich materials are typically synthesized by methods that include chemical vapor deposition [11], hydrothermal carbonization [12], and arc discharge [13]. However, the use of such methods requires sophisticated instruments that have a high energy consumption. An alternative simple method to make carbons is via flame pyrolysis, in which waste materials such as waste cooking oil can be used as a carbon source to produce onion-like nanocarbons (OLNCs) [14]. OLNCs are related to the family of carbon fullerenes [15]. They have a graphitic core, abundant surface functional groups, moderate porosity, and can have an inner cavity [16].

In this study, OLNCs were added to TiO_2 to form nanocomposites (TiO_2/OLNC) for use in the photodegradation of a model complex: methyl orange (MO). Zhang et al. reported that the combination of OLNCs and TiO_2 as photocatalysts was highly effective in the degradation of rhodamine B. This was attributed to the ability of the OLNCs to decrease the band gap of TiO_2, and to foster the decrease in the recombination of photo-generated electrons and holes [6]. The difference between this and the OLNCs reported in this study is that they were synthesized from waste cooking oil as a carbon source.

The model dye for this study was MO, as many studies have been done on this dye, and this allows for a comparison of the use of OLNCs with other carbons. This was done by comparing pristine TiO_2 with TiO_2/OLNC nanocomposites made with varying ratios of the TiO_2/OLNC.

2. Materials and Methods

2.1. Preparation of the OLNCs

All chemicals were purchased from Sigma Aldrich, South Africa, and were used as received. The waste cooking oil was collected from a local restaurant and used as received. The oil was subjected to flame pyrolysis in a method previously described [14]. In the reaction, a wick was filled with olive oil, which was placed in a flask containing waste

cooking oil (100 mL), and the wick was ignited with a flame. A bronze plate was used to collect the black soot, which consisted of OLNCs.

2.2. Synthesis of the Nanocomposites

The OLNCs (10 mg, 20 mg, 30 mg, and 50 mg) were added to 100 mg of TiO_2 (99.8% trace metals basis) in 50 mL of 5 M NaOH (reagent grade, ≥98%). The mixture was refluxed for 6 h at 100 °C. The product was separated from the solution using centrifugation and then rinsed with ethanol (95% analytical grade) and HCl (37% ACS reagent) to remove unreacted materials. The material was finally rinsed with distilled water and vacuum dried at 60 °C for 24 h.

The material was subjected to calcination at 450 °C for 4 h in an inert environment and called TC-10, TC-20, TC-30, and TC-50, according to the mass (mg) of OLNCs added to the TiO_2 (i.e., C:TiO_2 molar ratios of 1:2, 1:4, 1:6, and 1:10, respectively). The C content of the composites was determined from XPS data (see Tables S1 and S2). Adsorption studies were performed using MO (85% ACS reagent) as a model adsorbate. The adsorption of MO was studied using the OLNCs, and the nanocomposites were studied under constant conditions (pH = 7, solution volume 50 mL, the mass of adsorbent = 100 mg, for 120 min). The pH 7 was selected to mimic wastewater from the textile industry, which normally has a pH range from 7 to 12, and the pH_{PZC} of the TiO_2-OLNCs nanocomposites was around pH 8. Below pH 8, the composites would be protonated, resulting in an electrostatic attraction between the catalyst and the anionic dye (methyl orange).

2.3. Adsorption and Photocatalytic Experiments

The photocatalytic degradation of MO was conducted in a 100 mL quartz tube. The quartz tube was connected to a 300 W Xe short arc lamp (solar simulator equivalent to 1 sun radiation) as a source of light. In the reactions, 100 mg of the nanocomposite catalyst was introduced into 100 mL of 10 mg/L of MO solution at pH 7. Aliquots were withdrawn from the solution at appropriate intervals for analysis.

The experiment was first conducted in the dark for 30 min to determine the effect of any background illumination effects on the adsorption-desorption reaction. Then, the lamp was switched on, and 2 mL aliquots were withdrawn from the reaction mixture at 5, 10, 15, 20, 30, 60, and 120 min intervals. The final concentration of MO was determined by ultraviolet-visible (UV–Vis) spectroscopy, using a Cary 100 spectrophotometer at a wavelength of 465 nm.

Equation (1) was used to calculate the %degradation of methyl orange and Equation (2) (Langmuir–Hinshelwood kinetic model) was used to estimate the kinetic rate.

$$\%\text{Degradation} = \frac{C_O - C_e}{C_O} \times 100 \quad (1)$$

$$\text{Ln}\frac{C_O}{C_t} = K_{app} \times t \quad (2)$$

where C_O and C_e are the initial and equilibrium concentration of methyl orange, t is time (min), C_t is the concentration at any time, t and K_{app} is the rate constant.

2.4. Characterisation of the Photocatalytic Nanocomposites

A Micrometrics Tristar 3000 surface area and porosity analyzer was used to measure the surface area, pore size, and pore volume of the samples. For the thermal analysis of all the photocatalysts, a Perkin Elmer 6000 thermogravimetric analyzer was used, under air. A Bruker D2 Phaser Powder X-ray diffractometer operating with monochromatic Cu K_{alpha} radiation, generated at 10 mA and 30 kV, was used for determining the crystallinity of the nanocomposites. The morphological characteristics of the new materials were determined using scanning electron microscopy (SEM, ZEISS GeminiSEM 560 at sub 1 kV) and transmission electron microscopy (TEM; Jeol JEM-2100F 200 kV). The Thermo

ESCAlab 250Xi X-ray photoelectron spectroscopy (XPS) was used for elemental composition. The T64000 Raman spectrometer (HORIBA scientific, Jobin Yvon Technology, Oberursel, Germany) was used for studying the structural properties of the materials.

3. Results and Discussion

3.1. Characterization of the Photocatalytic Nanocomposites

3.1.1. Raman Spectroscopy

The Raman spectra of all the photocatalysts synthesized via the hydrothermal method are presented in Figure 1. The characteristic peaks of OLNCs are represented by the D band (1352 cm^{-1}) and the G band (1599 cm^{-1}). These peaks can be seen from all the composite (TiO_2/OLNCs) material, and not for the pure TiO_2. Characteristic peaks for pure TiO_2 can be seen at positions 653, 538, 404, and 218 cm^{-1}—they correspond with the presence of the anatase phase TiO_2 [17]. The aforementioned peaks appear in all the composite (TiO_2-OLNC) materials but not the clean OLNCs.

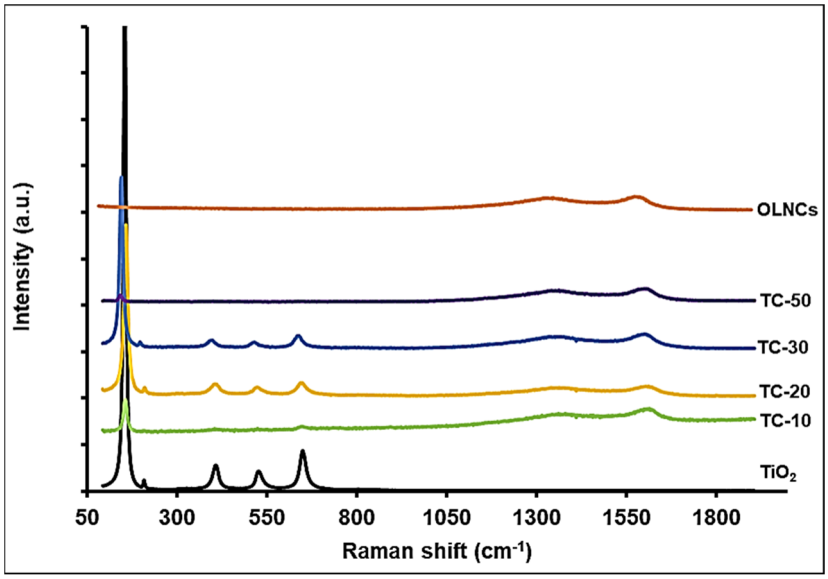

Figure 1. Raman spectra for all photocatalysts.

It is notable that the D band, G band, and the TiO_2 peaks shifted towards the lower frequency—an indication of tensile stress, as the TiO_2 interacted with the functional groups of the OLNCs [18]. The presence of the anatase phase TiO_2 was confirmed by the PXRD data (see Supplementary Figure S1) [19].

XPS data for the TC-10 material also showed the presence of TiO_2 (see Supplementary Figure S2 and Table S1) [20]. XPS survey spectra show all the characteristic peaks of a TiO_2-carbon composites material, with peaks at 284.7 eV (C1s), 531.1 eV (O1s), and 458.9 eV (Ti_{2p}) (Figure S2a). This indicates that the elemental composition of the photocatalyst consists of C, O, and Ti [3]. The XPS data were deconvoluted and the C, Ti, and O spectra are shown in Figure S2b, S2c, and S2d, respectively. The deconvoluted peak positions and intensities are given in Table S2. The Ti peak occurs at 458.9, corresponding to Ti in oxidation state 4^+, typical of a Ti-O bond. No indication of Ti-C bonding was observed (or expected). The C peak region showed the presence of C=C (13.9%), C-C (32.8%), and C-O/C=O (9.8%) bonds. The XPS O spectral region showed that O was in different environments typical of C=O (6.3%), (C-O) (6.7%), and TiO_2 (8.3%Ti; 17.3% O)). These results agree with the Raman and PXRD data, and are consistent with the synthesis of a TiO_2-OLNC composite.

Therefore, in this study, we have successfully synthesized a TiO_2-ONLC nanocomposite.

3.1.2. Thermogravimetric and Differential Thermal Analysis

Figure 2 shows the thermal decomposition steps for the photocatalysts, as the mass of the OLNCs was increased from 10 to 50 mg. From Figure 2a, two major weight loss steps can be seen for all the materials. The first weight loss took place at around 100 °C, and can be attributed to the evolution of moisture, which contributed 3% to 6% (TC-50, 5%; TC-30, 3%; TC-20 4%; TC-10; 6%) of the weight loss for the respective photocatalysts. The second major weight loss took place at 478 °C (TC-50), 480 °C (TC-30), 561° (TC-20), and 500 °C (TC-10), corresponding to 36%, 27%, 25%, and 13% weight loss for the respective materials, and can be attributed to the decomposition of organic material due to the carbon oxidation process [6]. The DTA thermograms give a clearer picture of the decomposition steps that all the nanocomposites underwent (Figure 2b). The remaining residue was TiO_2, and the analysis data confirmed the approximate TiO_2/OLNC ratios. The composites with the lower OLNCs content (TC-20 and TC-10) showed higher thermal stability than the composites with higher OLNCs content. However, pristine OLNCs (from our previous study) showed higher thermal stability (ca. 650 °C) than the as-synthesized TiO_2/OLNCs [14]. The hydrothermal treatment in the presence of NaOH affected the thermal stability of all of the nanocomposites [21].

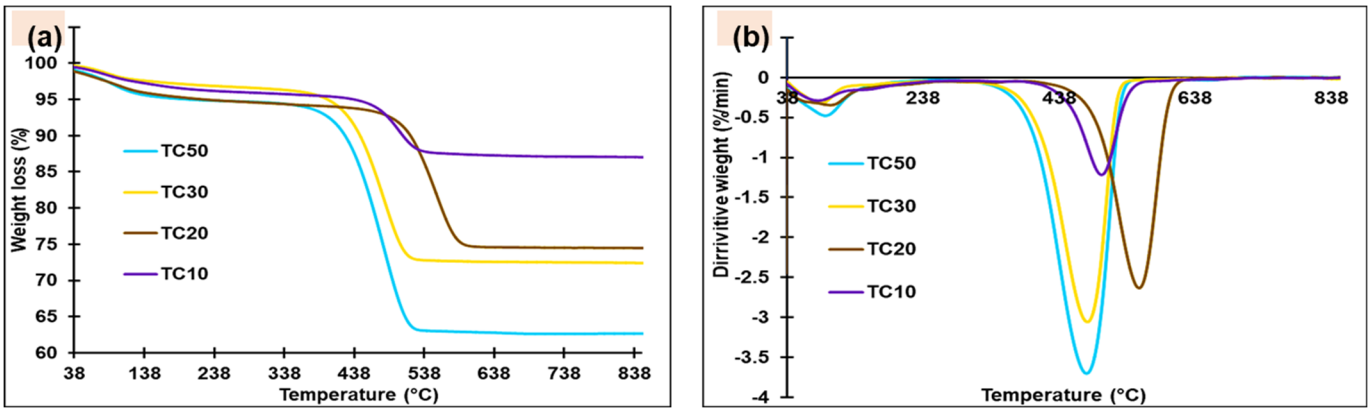

Figure 2. TGA (**a**) and DTA (**b**) thermograms for the TC-50, TC-30, TC-20, and TC-10 nanocomposites.

3.1.3. Morphological Characteristics and BET Analysis

The SEM micrographs for the TC-50, TC-30, TC-20, and TC-10 nanocomposites are shown in Figure 3. An irregular morphology can be observed in Figure 3a,b, which was similar to that reported by Da Dalt et al. for multiwall carbon nanotube-TiO_2 composites [22]. Contrary to this, Figure 3c,d showed quasi-spherical agglomerates consistent with the OLNCs morphology [23].

The TEM micrographs of all of the nanocomposites are shown in Figure 4. The images show that the material is quasi-spherical and multi-layered, and resembles that of an onion, as seen from all the nanocomposites. This is consistent with the morphology reported by Sikeyi et al. [23]. It can be seen that as the mass of OLNCs increased, the shape of the TiO_2 became more irregular. The TC-50 material shows lumps of irregular spheres (Figure 4a). When the mass of OLNCs is decreased to 30 mg (TC-30), the morphology of the TiO_2 consists of irregular spheres with a spider web connection (Figure 4b). The TiO_2 transforms into a tube-like nanostructure when the mass of the OLNCs is decreased to 20 mg (TC-20) (Figure 4c). Similar morphology is seen when the mass of the OLNCs is decreased to 10 mg (TC-10) (Figure 4d). Such a morphology of the TiO_2 is familiar to the titania made in alkaline media, e.g., in synthesized TiO_2 (titanate) nanotubes [24]. Wang et al. reported that the conversion of anatase to titanate could be hindered by the presence of a carbon layer [25]. This may be the case in this study, as the occurrence of nanotubes disappears in the material with higher carbon mass, as seen in the TC-30 and TC-50 materials.

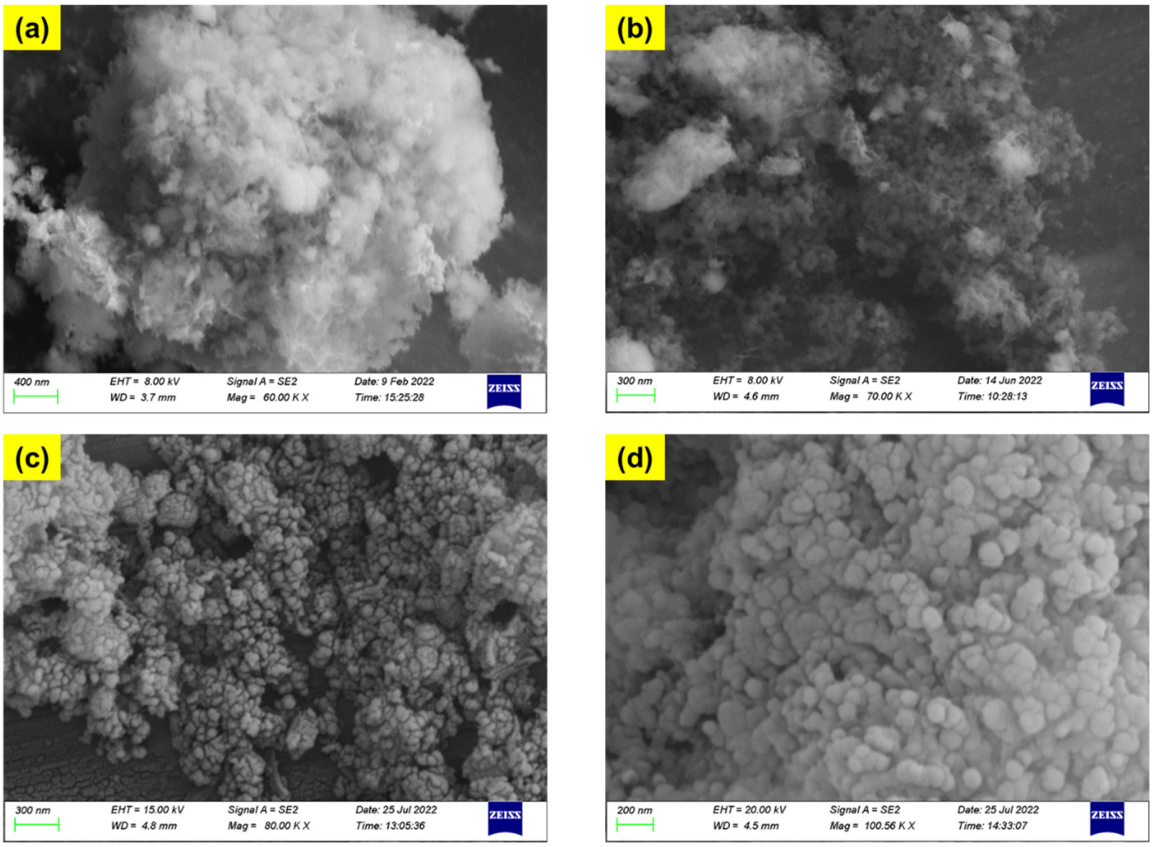

Figure 3. SEM micrographs for the TC-10 (**a**), TC-20 (**b**), TC-30 (**c**), and TC-50 (**d**) nanocomposites.

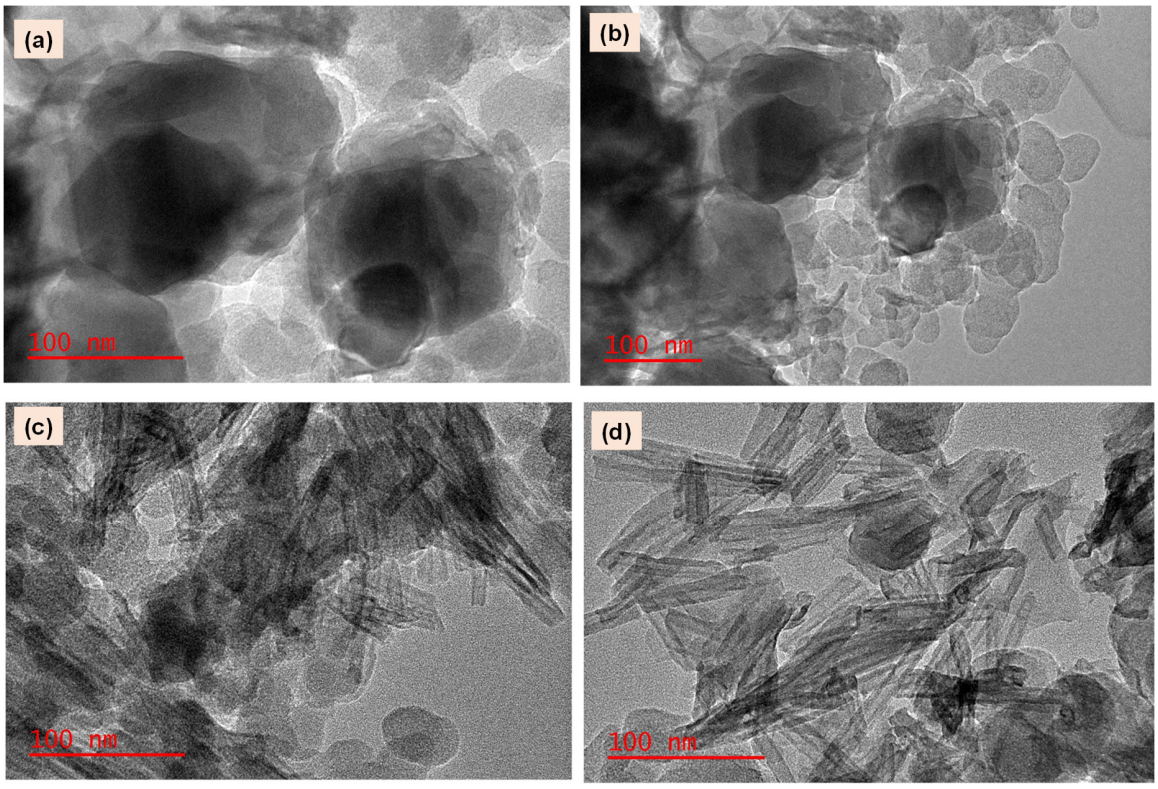

Figure 4. TEM micrographs for the TC-50 (**a**), TC-30 (**b**), TC-20 (**c**), and TC-10 (**d**) nanocomposites.

The surface area of the nanocomposites was considerably higher than that of pure TiO_2, in the order TiO_2 (7 m^2/g) < TC-10 (56 m^2/g) < TC-20 (69 m^2/g) < TC-30 (78 m^2/g) < TC-50 (120 m^2/g). This suggests that the addition of the OLNCs contributed to the increased surface area, since OLNCs alone (80.89 m^2/g) [14] have a higher surface area compared to the as-prepared TiO_2 (Table 1). The pore volume and average pore size were also increased by the addition of the OLNCs, but did not show any particular trend.

Table 1. BET parameters for TiO_2 and the OLNCs/TiO_2 nanocomposite.

Adsorbent	Surface Area (m^2/g)	Pore Volume (cm^3/g)	Average Pore Size (nm)
TiO_2	7.6	0.02	7.58
TC-10	56.6	0.12	8.09
TC-20	69.8	0.19	10.80
TC-30	78.1	0.17	8.85
TC-50	120	0.28	9.43

3.1.4. Optical Characteristics

The optical properties of the as-synthesized photocatalysts were studied using ultraviolet-visible spectroscopy (Figure 5). It can be seen that as the mass of the OLNCs increased from 10 mg to 50 mg, and the absorption band of the materials is similar (Figure 5a). This gives the calculated bandgap energies of all the photocatalysts (~3.2 eV), which is similar to that of pure TiO_2 (Figure 5b–f) [26]. This result is different from that of Zhang et al., who reported a bandgap of 2.094 eV CNOs/TiO_2 composite [6].

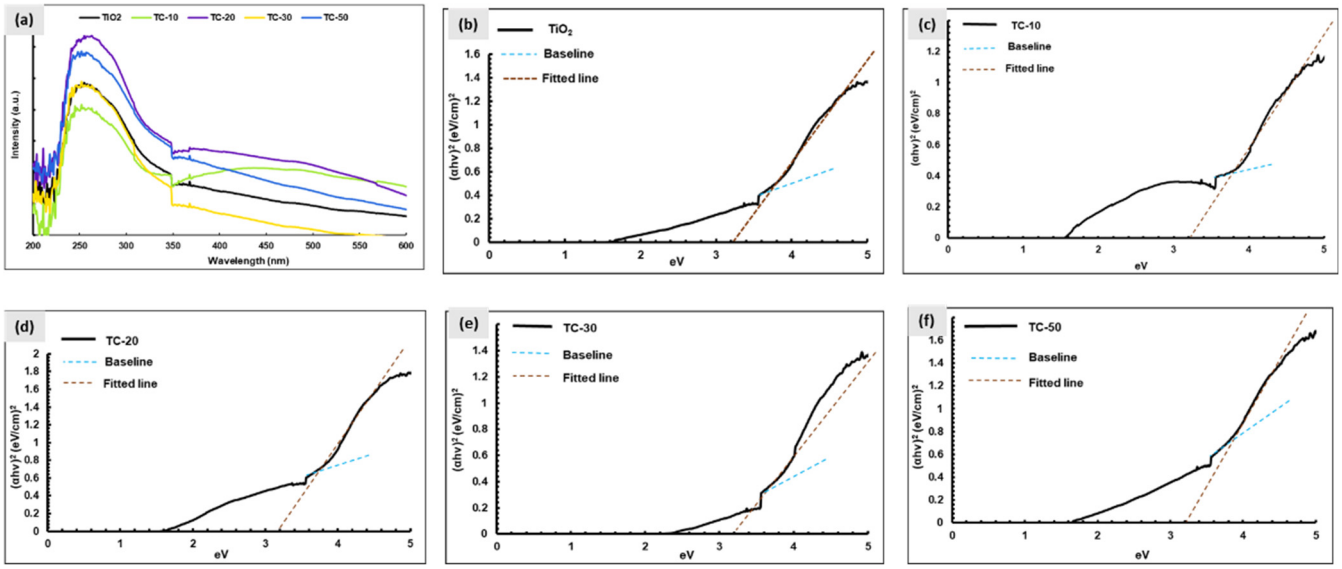

Figure 5. UV-Vis spectroscopy scanning (**a**) of all the materials and bandgap energies for TiO_2 (**b**), TC-10 (**c**), TC-20 (**d**), TC-30 (**e**), and TC-50 (**f**) photocatalysts.

3.2. Photocatalytic Degradation of Methyl Orange

The photocatalytic degradation of MO was evaluated using TiO_2 and the TiO_2/OLNCs nanocomposites (Figure 6). The reaction was first conducted in the absence of any photocatalyst, first in the dark for 30 min, and 120 min under light irradiation. Only a small amount of photodegradation of the MO (120 min) was observed in the absence of the photocatalyst.

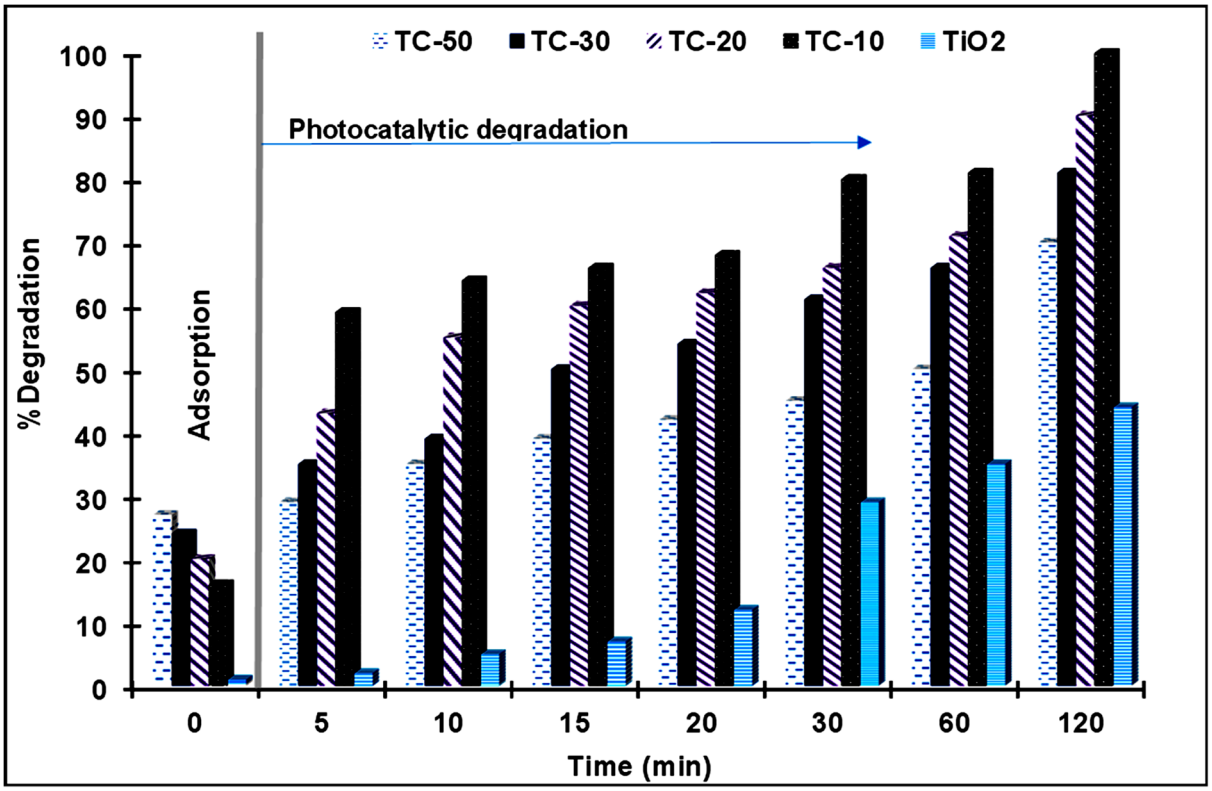

Figure 6. Photocatalytic degradation of MO using TiO_2, TC-50, TC-30, TC-20, and TC-10 photocatalysts.

A similar experiment was performed with TiO_2 in the dark, and an insignificant amount of MO was degraded. However, as expected, the TiO_2 catalyst was able to photodegrade the MO under light irradiation, with 44% of MO degraded after 120 min (Figure 6). The photocatalytic degradation of MO was then carried out with the composites (TiO_2/OLNC). When the experiment was carried out in the dark, it was noted that all composites showed adsorption of the dye. Furthermore, as the OLNC content increased, the adsorption efficiency also increased. This suggests that the OLNCs assist with the MO adsorption process [22]. This is in line with the increased surface area as the mass of OLNCs increased, as shown in Table 1.

However, the best photocatalytic result was found to be the composite with the lowest loading of OLNCs (Figure 6). This suggests that two effects are at play: (i) at low loadings, the OLNCs enhance the conductivity; but (ii) at high loadings, the carbon covers the active TiO_2 sites, i.e., the OLNCs cover the photoactive sites of the TiO_2, resulting in a decreased light transmittance and charge transfer, indicating that the surface area was not the major driving force in the photocatalytic degradation of MO [22].

Similar observations were made by Zhang et al. for the CNOs/TiO_2 composites used for the degradation of rhodamine B. It was reported that the composite that showed the most effective photocatalytic activity was the composite with a 10% mass ratio of CNOs to TiO_2, due to the increased adsorption capacity of the composites compared to the bare TiO_2 (see Table S3), as calculated by Equation (S1).

Figure S3 depicts the Langmuir (Equation (S2)) and Fruendlich (Equation (S3)) adsorption isotherms, which were selected to study the adsorption process. It can be seen from the figures that the experimental data fitted the Langmuir model for all the composite materials. This possibly indicates that the adsorption of the methyl orange was through a homogeneous surface coverage. Interestingly, for the bare TiO_2 material, the experimental data fitted the Fruendlich adsorption isotherm, possibly indicating that the adsorption pathway was through a heterogeneous surface coverage. The adsorption pathway was also studied using the intra-particle diffusion model, by plotting q_t vs. $t^{1/2}$, as shown

in Figure S4. It can be seen that all the catalysts show multiple linear regions that do not pass through the origin point. This indicates that the adsorption pathway involves a multiple-step mechanism. This involves (a) a bulk transport, as the catalyst is in contact with the dye; (b) film diffusion, where the dye molecules are transported to the boundary layer or film of the catalyst; and then (c) intra-particle diffusion of the dye molecules into the catalyst pores. The last step (d) involves the adsorption of the dye molecules onto the adsorption sites of the catalyst [27].

3.3. Kinetics

The kinetics of the photocatalytic degradation of MO using TiO_2 and its composites were evaluated (Figure 7; Table 2). The experimental data fitted the first-order kinetic model. The photocatalytic degradation of MO was improved by the addition of OLNCs on the surface of the TIO_2. This was attributed to the enhanced adsorptivity of the OLNCs, which resulted in adsorption-coupled photocatalytic degradation synergy between the ONLCs and the TiO_2 [28]. As with the conversion data, the kinetic results followed the same trends of faster rates in the order 10 mg > 20 mg > 30 mg > 50 mg > TiO_2. This can be attributed to decreased electron-hole recombination due to the addition of OLNCs [22]. The TC-10 photocatalyst was selected for further study, as it gave the best performance.

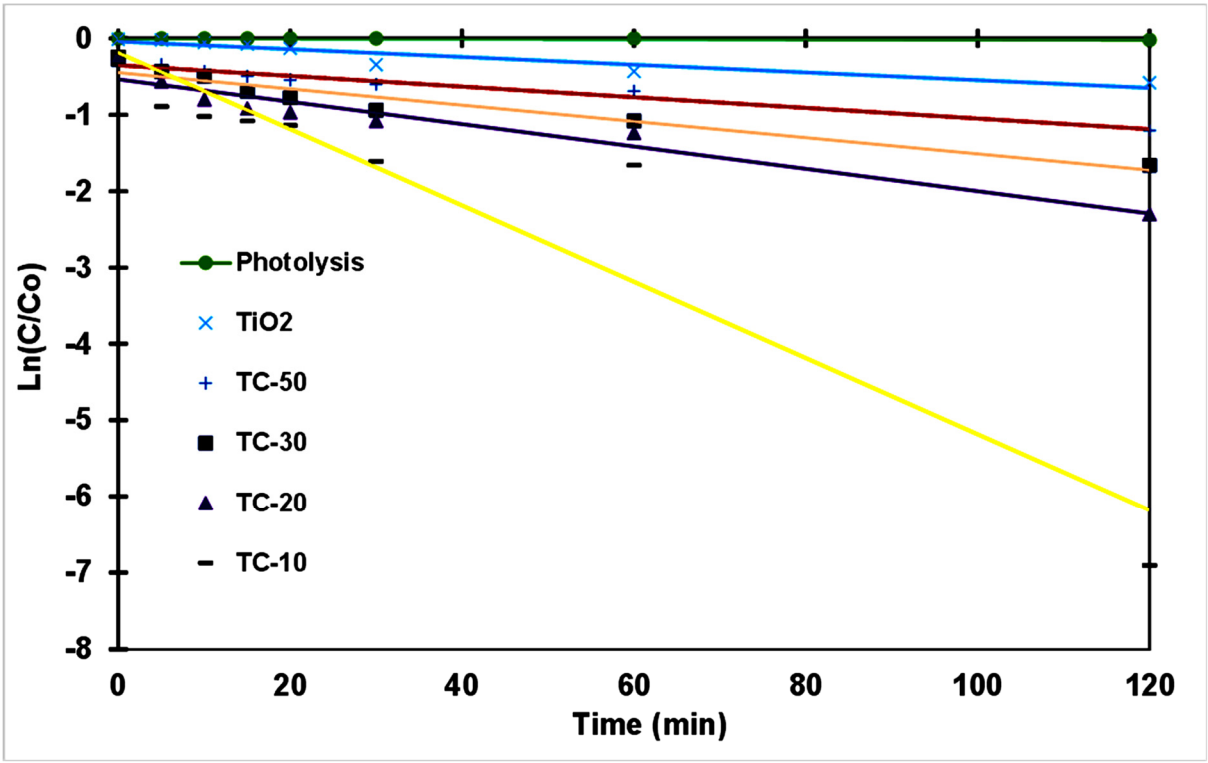

Figure 7. First-order kinetics of the photocatalytic degradation of methyl orange.

Table 2. Parameters for the first-order kinetics for the photocatalytic degradation of methyl orange.

Photocatalyst	Equations	R^2	k (min^{-1})
TiO_2	$Ln(C/C_o) = -0.0051X - 0.0395$	0.8745	0.005
TC-50	$Ln(C/C_o) = -0.007X - 0.3511$	0.9728	0.007
TC-30	$Ln(C/C_o) = -0.00106X - 0.4488$	0.9307	0.001
TC-20	$Ln(C/C_o) = -0.0146X - 0.5349$	0.9229	0.015
TC-10	$Ln(C/C_o) = -0.05X - 0.1861$	0.8975	0.050
TC-10 (H_2O_2)	$Ln(C/C_o) = -0.287X + 0.6119$	0.9002	0.287

The photocatalytic degradation of MO was investigated in the presence of 5% H_2O_2 (Figure 8). It can be seen that complete degradation of MO was observed in 30 min of light irradiation (Figure 8a), with a first-order kinetic rate of 0.287 min^{-1} (Table 2 and Figure 8b). The kinetic rate was six times faster than the 0.050 min^{-1} that took place in the absence of H_2O_2. The ability of H_2O_2 to decrease the electron-hole recombination reaction could be because of the process of harvesting the electrons and producing more hydroxyl radicals [29].

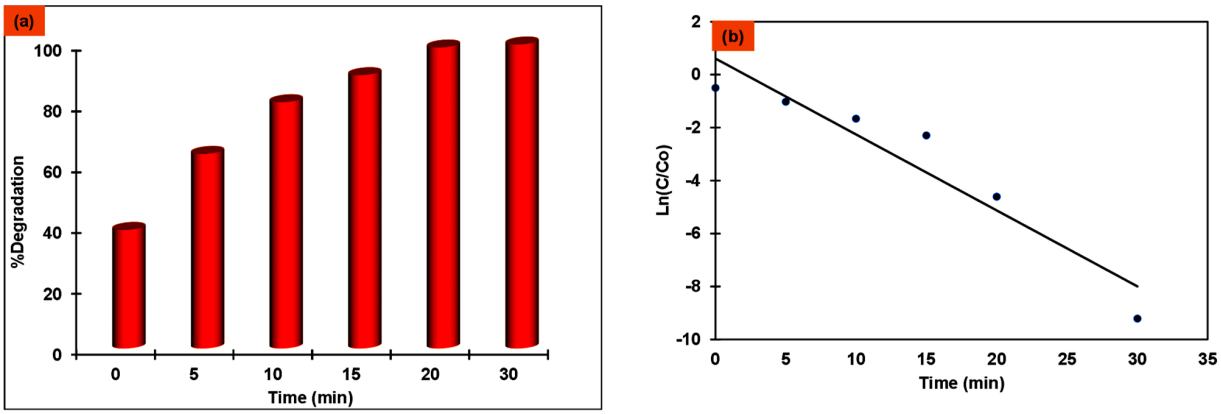

Figure 8. The photocatalytic degradation (**a**) and first-order kinetic curve (**b**) for the TC-10 photocatalyst in the presence of 5% H_2O_2.

3.4. Methyl Orange Speciation and the Regeneration of the Photocatalyst

Figure 9 shows the removal of MO by the TC-10 photocatalyst. The absorption spectrum depicts a maximum absorption peak at ~465 nm, which decreased as the photocatalytic degradation progressed from 5 min to 120 min. The color of the MO solution changed from orange to colorless. No new peaks were observed throughout the reaction, indicating that there was no formation of any chromophoric compounds [30].

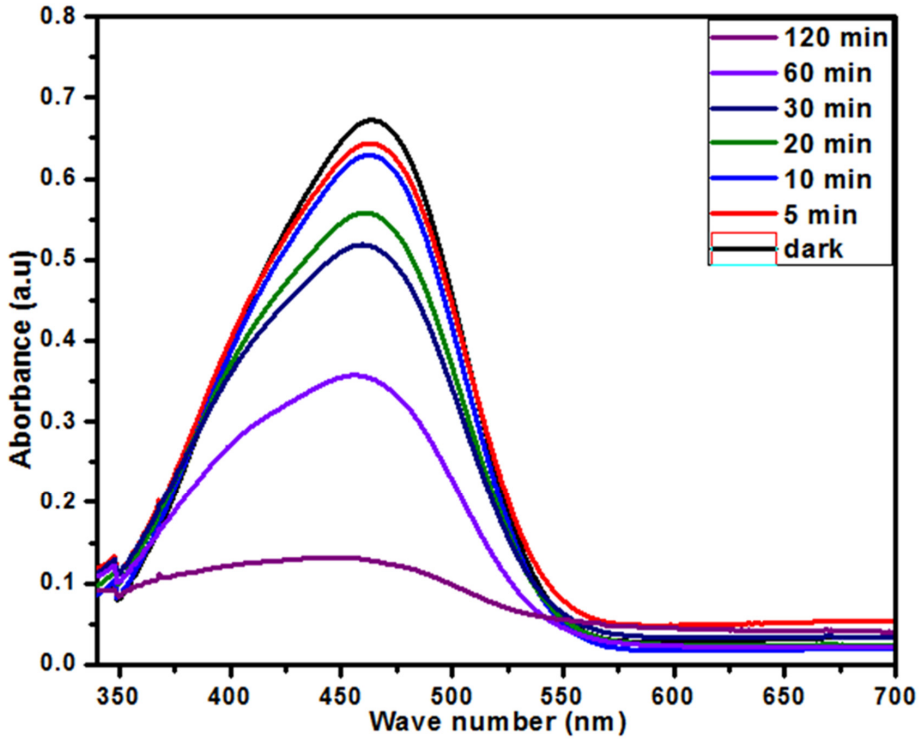

Figure 9. Absorption spectra of methyl orange, as degraded by TC-10 over time.

The photocatalyst's recyclability was evaluated by first conducting photocatalytic experiments for the degradation of MO for 120 min at neutral pH. Thereafter, the photocatalyst was separated from the solution by centrifugation. This was followed by rinsing the catalysts with 0.1 M NaOH and then boiling water to leach out any MO that may have been adsorbed on the surface of the photocatalyst. The photocatalyst was then dried at 60 °C for 24 h and was reused in the photocatalytic degradation of more methyl orange. This process was performed five times, with the results presented in Figure 10. The activity decreased with reuse: 100% > 95% > 89% > 81% > 76%. This was attributed to the loss of mass each time it was reused [6].

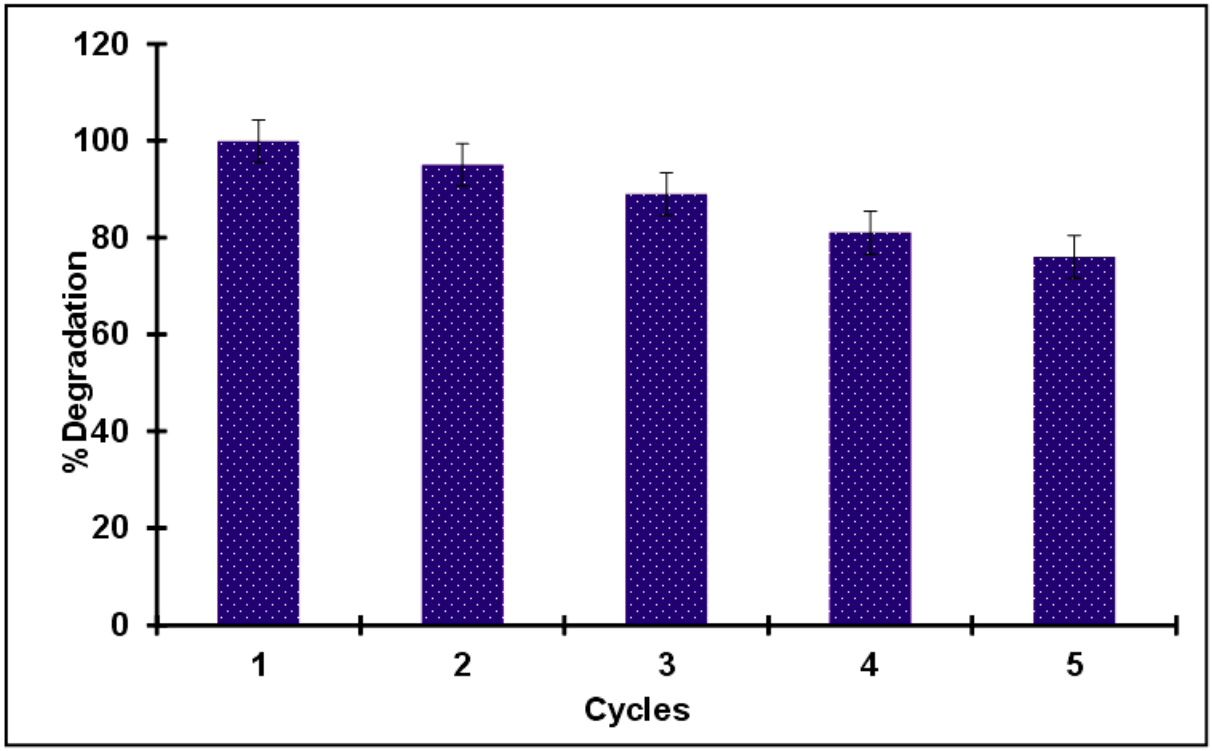

Figure 10. Regeneration of the TC-10 photocatalyst over five cycles of MO photocatalytic degradation.

3.5. Possible Degradation Mechanism

Figure 11 is an illustration of the proposed degradation mechanism of MO using the OLNCs/TiO_2 nanocomposite as a photocatalyst. The mechanism is based on the literature for similar carbon-TiO_2 composites [31]. At first, the MO ions are adsorbed on the surface of the nanocomposite through the carbonyl groups [32]. This was followed by light irradiation and the photo generation of electrons (e^-). As the e^- migrates from the valence band (VB) to the conduction band (CB), holes (h^+) are created in the VB. The TiO_2 will then donate an e^- to the OLNCs, thus preventing the rapid recombination of e^-/h^+. The e^- reacts with O_2 to form oxide radicals ($O2^-$) on the surface of the nanocomposite, simultaneously forming hydroxyl radicals (·OH) in the VB. Lastly, the respective radicals would degrade the MO.

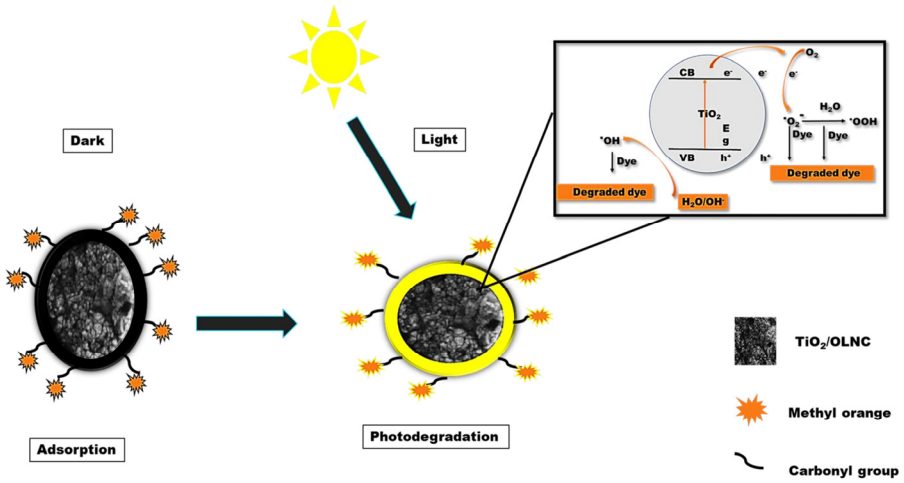

Figure 11. Schematic representation of MO degradation using the OLNCs/TiO_2 photocatalyst.

3.6. Comparison with Other Carbon/TiO_2 Composites

A comparison of different carbon nanomaterials in composites with TiO_2 for the photocatalytic degradation of MO is presented in Table 3. A direct comparison is difficult due to differences in the experimental conditions used by the different workers. In Table 3, different composites of TiO_2/carbon nanomaterials with different sources of carbon are presented: carbon nanofibers [CNFs] of cellulose origin (TiO_2/CNF), graphitic carbon nitride (g-C_3N_4: TiO_2/g-C_3N_4), nitrogen-doped graphene quantum dots (N-GQDs) [N-GQD/TiO_2], carbon quantum dots (CQDs) [TiO_2/CQD], multiwall-carbon nanotubes (MWCNTs) [MWCNT/TiO_2], and OLNCs [TiO_2/OLNC].

In all cases, the combination of carbon/TiO_2 has proven effective in the removal of MO at low initial concentrations (10 to 40 mg/L). The adsorption of MO to the photocatalyst's surface is important for the rapid degradation of the dye. For the selected composites, adsorption of the dye by the TiO_2 alone was lower than in the composite materials. This was attributed to the active sites responsible for dye adsorption. This resulted in a synergistic removal pathway of the dye with the dye adsorbed on the surface of the photocatalyst through carbon material. This was followed by the degradation of the dye molecules through the TiO_2. The synthesized composites of TiO_2/OLNC proved to be comparable with other carbon/TiO_2-based photocatalysts, as it demonstrates 99.9% degradation of MO at 120 min—significantly higher than all the presented composites. However, the TiO_2/CNF and the MWCNT/TiO_2 showed fewer reaction times of 30 min and 90 min, respectively, with the TiO_2/CNF having the lowest volume of MO solution (20 mL). The composites with the lowest degradation were the TiO_2/CQD and TiO_2/g-C_3N_4 at 39.1% and 55%, respectively. This could be due to the generally low surface functional groups [33]. Therefore, along with a simple synthesis method of flame pyrolysis of waste cooking oil for making OLNCs the TiO_2/OLNC composites show potential in the photocatalytic degradation of MO.

Table 3. Comparison of different carbon/TiO_2 photocatalysts for MO degradation.

Photocatalyst	Carbon Source	C_O (mg/L)	Degradation (%)	Time (Min)	Volume (mL)	Reference
TiO_2/CNF	Nanocellulose	40	99.72	30	20	[34]
TiO_2/g-C_3N_4	g-C_3N_4	10	55	180	100	[35]
N-GQD/TiO_2	N-GQDs	10	95	120	50	[36]
TiO_2/CQD	CQDs	10	39.1	120	100	[37]
MWCNT/TiO_2	MWCNTs	15	97.4	90	150	[38]
TiO_2/MC	RF	100	89	75	*	[39]
Ag/TiO_2/biochar	Biochar	20	97.48	60	40	[40]
TiO_2/OLNC	OLNCs	10	99.9	120	100	This study

* No data provided.

4. Conclusions

This study has demonstrated the synthesis of OLNCs from the flame pyrolysis of waste cooking oil. This resulted in high-quality carbon nanomaterial composites (TiO_2/OLNC), where the amount of OLNCs was varied (10 mg, 20 mg, 30 mg, and 50 mg). The nanocomposites were effective in the photocatalytic degradation of MO compared to TiO_2 alone, with the TC-10 material having the faster kinetic rate. This was attributed to synergy between TiO_2 and the OLNCs.

The addition of H_2O_2 greatly enhanced the photocatalytic activity of the photocatalyst due to the harvesting of electrons by the H_2O_2, thus limiting recombination. No formation of chromophoric compounds was detected when the as prepared photocatalysts were applied in the degradation of methyl orange. Overall, the TiO_2/OLNCs nanocomposites have potential to be applied as photocatalysts for MO degradation. This was achieved by converting a waste material (waste cooking oil) to onion-like nanocarbons, which were added to TiO_2. This allowed for better photocatalytic activity for the nanocomposites than pure TiO_2, due to enhanced adsorption capability. The study has shown that nanocomposites of OLNCs/TiO_2 are potential photocatalysts for the photocatalytic degradation of methyl orange.

Supplementary Materials: The following supporting information can be downloaded at: https://www.mdpi.com/article/10.3390/app13085125/s1, Figure S1: PXRD patterns of anatase TiO_2 phase for TC-10, TC-20, TC-30, and TC-50. Figure S2: XPS survey spectra of TC-10 photocatalyst (a), deconvoluted spectra for Ti (b), C (c) and O (d) respectively. Figure S3: Linear plots for Langmuir isotherm TC-10 (a), TC-20 (b), TC-30 (c), TC-50 (d) and the Fruendlich isotherm TiO_2 (e). Figure S4: Intra-particle diffusion plots for all the catalysts TC-10 (a), TC-20 (b), TC-30 (c), TC-50 (d) and TiO_2 (e). Table S1: Elemental identification and quantification. Table S2: Data from the deconvoluted XPS spectra. Table S3: Adsorption capacity of all the photocatalysts.

Author Contributions: T.D.N.: conceptualization, methodology, writing—original draft, investigation, formal analysis, writing—review and editing, validation. L.L.S.: data curation, formal analysis, investigation. F.D.: data curation, formal analysis, investigation. N.J.C.: supervision, resources, writing—review and editing, validation. E.N.N.: supervision, resources, writing—review and editing, validation. M.S.M.-N.: conceptualization, supervision, resources, project administration, writing—review and editing, validation. All authors have read and agreed to the published version of the manuscript.

Funding: This work was supported in part by the National Research Foundation of South Africa (Grant number: 138075), the University of the Witwatersrand and the DSI-NRF Centre of Excellence in Strong Materials (CoESM). The authors would like to acknowledge Siyasanga Mpelane (University of Johannesburg, Auckland Park) for the high magnification TEM analysis.

Institutional Review Board Statement: The study did not require ethical clearance.

Informed Consent Statement: Not applicable.

Data Availability Statement: The data presented in this study are available on request from the corresponding author. The data are not publicly available due to privacy.

Conflicts of Interest: The authors report no conflict of interest.

References

1. Li, J.; You, J.; Wang, Z.; Zhao, Y.; Xu, J.; Li, X.; Zhang, H. Application of α-Fe_2O_3-based heterogeneous photo-Fenton catalyst in wastewater treatment: A review of recent advances. *J. Environ. Chem. Eng.* **2022**, *10*, 108329. [CrossRef]
2. You, J.; Wang, L.; Bao, W.; Yan, A.; Guo, R. Synthesis and visible-light photocatalytic properties of BiOBr/CdS nanomaterials. *J. Mater. Sci.* **2021**, *56*, 6732–6744. [CrossRef]
3. You, J.; Wang, L.; Zhao, Y.; Bao, W. A Review of Amino-Functionalized Magnetic Nanoparticles for Water Treatment: Features and Prospects. *J. Clean. Prod.* **2021**, *281*, 124668. [CrossRef]
4. Naikwade, A.G.; Jagadale, M.B.; Kale, D.P.; Gophane, A.D.; Garadkar, K.M.; Rashinkar, G.S. Photocatalytic Degradation of Methyl Orange by Magnetically Retrievable Supported Ionic Liquid Phase Photocatalyst. *ACS Omega* **2020**, *5*, 131–144. [CrossRef] [PubMed]

5. Vu Nu, T.T.; Thi Tran, N.H.; Truong, P.L.; Phan, B.T.; Nguyen Dinh, M.T.; Dinh, V.P.; Phan, T.S.; Go, S.; Chang, M.; Loan Trinh, K.T.; et al. Green synthesis of microalgae-based carbon dots for decoration of TiO_2 nanoparticles in enhancement of organic dye photodegradation. *Environ. Res.* **2022**, *206*, 112631. [CrossRef] [PubMed]
6. Zhang, Y.; Zhang, W.; Yang, K.; Yang, Y.; Jia, J.; Liang, Y.; Guo, L. Carbon Nano-Onions (CNOs)/TiO_2 Composite Preparation and Its Photocatalytic Performance under Visible Light Irradiation. *J. Environ. Eng.* **2020**, *146*, 1–12. [CrossRef]
7. Mente, P.; Mashindi, V.; Phaahlamohlaka, T.N.; Monyatsi, T.N.; Forbes, R.P.; Coville, N.J. Oxidation of Benzyl Alcohol Using Cobalt Oxide Supported Inside and Outside Hollow Carbon Spheres. *ChemistryOpen* **2021**, *10*, 618–626. [CrossRef]
8. Mofokeng, T.P.; Tetana, Z.N.; Ozoemena, K.I. Defective 3D nitrogen-doped carbon nanotube-carbon fibre networks for high-performance supercapacitor: Transformative role of nitrogen-doping from surface-confined to diffusive kinetics. *Carbon N. Y.* **2020**, *169*, 312–326. [CrossRef]
9. Pakade, V.E.; Maremeni, L.C.; Ntuli, T.D.; Tavengwa, N.T. Application of quaternized activated carbon derived from Macadamia nutshells for the removal of hexavalent chromium from aqueous solutions. *S. Afr. J. Chem.* **2016**, *69*, 180–188. [CrossRef]
10. Mahmoodi, N.M. Photocatalytic degradation of dyes using carbon nanotube and titania nanoparticle. *Water Air Soil Pollut.* **2013**, *224*, 1612. [CrossRef]
11. Hussain, C.M. Carbon Nanomaterials as Adsorbents for Environmental Analysis. *Nanomater. Environ. Prot.* **2015**, *9781118496*, 217–236. [CrossRef]
12. Mkhari, O.; Ntuli, T.D.; Coville, N.J.; Nxumalo, E.N.; Maubane-Nkadimeng, M.S. A comparison of fluorescent N-doped carbon dots supported on the surface of hollow and solid carbon spheres, and solid silica spheres. *Diam. Relat. Mater.* **2021**, *118*, 108500. [CrossRef]
13. Sharma, R.; Sharma, A.K.; Sharma, V. Synthesis of carbon nanotubes by arc-discharge and chemical vapor deposition method with analysis of its morphology, dispersion and functionalization characteristics. *Cogent Eng.* **2015**, *2*, 1094017. [CrossRef]
14. Ntuli, T.D.; Mongwe, T.H.; Sikeyi, L.L.; Mkhari, O.; Coville, N.J.; Nxumalo, E.N.; Maubane-Nkadimeng, M.S. Removal of hexavalent chromium via an adsorption coupled reduction mechanism using olive oil derived carbon nano-onions. *Environ. Nanotechnol. Monit. Manag.* **2021**, *16*, 100477. [CrossRef]
15. Shaku, B.; Mofokeng, T.P.; Mongwe, T.H.; Coville, N.J.; Ozoemena, K.I.; Maubane-Nkadimeng, M.S. Physicochemical Properties of Nitrogen Doped Carbon Nano-onions Grown by Flame Pyrolysis from Grapeseed Oil for Use in Supercapacitors. *Electroanalysis* **2020**, *32*, 2946–2957. [CrossRef]
16. Sikeyi, L.L.; Ntuli, T.D.; Mongwe, T.H.; Maxakato, N.W.; Carleschi, E.; Doyle, B.P.; Coville, N.J.; Maubane-Nkadimeng, M.S. Microwave assisted synthesis of nitrogen doped and oxygen functionalized carbon nano onions supported palladium nanoparticles as hybrid anodic electrocatalysts for direct alkaline ethanol fuel cells. *Int. J. Hydrogen Energy* **2021**, *46*, 10862–10875. [CrossRef]
17. Chaudhary, D.; Khare, N.; Vankar, V.D. Ag nanoparticles loaded TiO_2/MWCNT ternary nanocomposite: A visible-light-driven photocatalyst with enhanced photocatalytic performance and stability. *Ceram. Int.* **2016**, *42*, 15861–15867. [CrossRef]
18. Ghos, B.C.; Farid, S.; Farhad, U.; Patwary, A.M.; Majumder, S.; Hossain, A.; Tanvir, N.I.; Rahman, M.A.; Tanaka, T. Influence of the Substrate, Process Conditions, and Postannealing Temperature on the Properties of ZnO Thin Films Grown by the Successive Ionic Layer Adsorption and Reaction Method. *ACS Omega* **2021**, *6*, 2665–2674. [CrossRef] [PubMed]
19. John, A.K.; Palaty, S.; Sharma, S.S. Greener approach towards the synthesis of titanium dioxide nanostructures with exposed {001} facets for enhanced visible light photodegradation of organic pollutants. *J. Mater. Sci. Mater. Electron.* **2020**, *31*, 20868–20882. [CrossRef]
20. Yu, W.; Zheng, B.; Mao, K.; Jiang, J.; Luo, B.; Wu, X.; Tao, T.; Min, X.; Mi, R.; Huang, Z.; et al. Interfacial structure and photocatalytic degradation performance of graphene oxide bridged chitin-modified TiO_2/carbon fiber composites. *J. Clean. Prod.* **2022**, *361*, 132261. [CrossRef]
21. Chen, H.; Wu, J.; Shi, J.; Zhang, W.; Wang, H. Effect of alkali treatment on microstructure and thermal stability of parenchyma cell compared with bamboo fiber. *Ind. Crops Prod.* **2021**, *164*, 113380. [CrossRef]
22. Da Dalt, S.; Alves, A.K.; Bergmann, C.P. Photocatalytic degradation of methyl orange dye in water solutions in the presence of MWCNT/TiO_2 composites. *Mater. Res. Bull.* **2013**, *48*, 1845–1850. [CrossRef]
23. Sikeyi, L.L.; Ntuli, T.D.; Mongwe, T.H.; Maxakato, N.W.; Coville, N.J.; Maubane-Nkadimeng, M.S. Platinum Nanoparticles Loaded on Pristine and Boron Oxide Modified Carbon Nano-Onions for Enhanced Ammonia Electrooxidation in Alkaline Direct Ammonia Fuel Cells. *J. Electroanal. Chem.* **2022**, *917*, 116411. [CrossRef]
24. Xiong, J.; He, L. Influence of Na+content on the structure and morphology of TiO_2nanoparticles prepared by hydrothermal transformation of alkaline titanate nanotubes. *J. Exp. Nanosci.* **2017**, *12*, 384–393. [CrossRef]
25. Wang, X.; Pan, H.; Xue, X.; Qian, J.; Yu, L.; Yang, J.; Zhang, Z. Preparation and characterization of titanate nanotubes/carbon composites. *Mater. Chem. Phys.* **2011**, *130*, 827–830. [CrossRef]
26. Fujishima, A.; Honda, K. Electrochemical photolysis of water at a semiconductor electrode. *Nature* **1972**, *238*, 37–40. [CrossRef]
27. Pholosi, A.; Naidoo, E.B.; Ofomaja, A.E. Intraparticle diffusion of Cr(VI) through biomass and magnetite coated biomass: A comparative kinetic and diffusion study. *S. Afr. J. Chem. Eng.* **2020**, *32*, 39–55. [CrossRef]
28. Xiong, L.; Lan, D.; Liang, H.; Chen, L.; Wang, Q. Grafting TiO_2 nanoparticles onto carbon fiber via "thiol-ene" click chemistry and its photodegradation performance for methyl orange. *Mater. Lett.* **2018**, *211*, 296–299. [CrossRef]
29. Rahmati, R.; Nayebi, B.; Ayati, B. Investigating the effect of hydrogen peroxide as an electron acceptor in increasing the capability of slurry photocatalytic process in dye removal. *Water Sci. Technol.* **2021**, *83*, 2414–2423. [CrossRef] [PubMed]

30. Park, S.J.; Das, G.S.; Schütt, F.; Adelung, R.; Mishra, Y.K.; Tripathi, K.M.; Kim, T.Y. Visible-light photocatalysis by carbon-nano-onion-functionalized ZnO tetrapods: Degradation of 2,4-dinitrophenol and a plant-model-based ecological assessment. *NPG Asia Mater.* **2019**, *11*, 8. [CrossRef]
31. Zhang, Y.; Hawboldt, K.; Zhang, L.; Lu, J.; Chang, L.; Dwyer, A. Carbonaceous nanomaterial-TiO_2 heterojunctions for visible-light-driven photocatalytic degradation of aqueous organic pollutants. *Appl. Catal. A Gen.* **2022**, *630*, 118460. [CrossRef]
32. Shah, S.S.; Sharma, T.; Dar, B.A.; Bamezai, R.K. Adsorptive removal of methyl orange dye from aqueous solution using populous leaves: Insights from kinetics, thermodynamics and computational studies. *Environ. Chem. Ecotoxicol.* **2021**, *3*, 172–181. [CrossRef]
33. Khojasteh, H.; Salavati-Niasari, M.; Safajou, H.; Safardoust-Hojaghan, H. Facile reduction of graphene using urea in solid phase and surface modification by N-doped graphene quantum dots for adsorption of organic dyes. *Diam. Relat. Mater.* **2017**, *79*, 133–144. [CrossRef]
34. Liu, G.Q.; Pan, X.J.; Li, J.; Li, C.; Ji, C.L. Facile preparation and characterization of anatase TiO_2/nanocellulose composite for photocatalytic degradation of methyl orange. *J. Saudi Chem. Soc.* **2021**, *25*, 101383. [CrossRef]
35. Zang, Y.; Li, L.; Xu, Y.; Zuo, Y.; Li, G. Hybridization of brookite $TiO_2$with g-C3N4: A visible-light-driven photocatalyst for As3+oxidation, MO degradation and water splitting for hydrogen evolution. *J. Mater. Chem. A* **2014**, *2*, 15774–15780. [CrossRef]
36. Pan, D.; Jiao, J.; Li, Z.; Guo, Y.; Feng, C.; Liu, Y.; Wang, L.; Wu, M. Efficient separation of electron-hole pairs in graphene quantum dots by TiO_2 heterojunctions for dye degradation. *ACS Sustain. Chem. Eng.* **2015**, *3*, 2405–2413. [CrossRef]
37. Zhang, X.; Li, Z.; Xu, S.; Ruan, Y. Carbon quantum dot-sensitized hollow TiO_2 spheres for high-performance visible light photocatalysis. *New J. Chem.* **2021**, *45*, 8693–8700. [CrossRef]
38. Ouyang, K.; Xie, S.; Ma, X. Photocatalytic activity of TiO_2 supported on multi-walled carbon nanotubes under simulated solar irradiation. *Ceram. Int.* **2013**, *39*, 7531–7536. [CrossRef]
39. Yin, B.; Wang, J.T.; Xu, W.; Long, D.H.; Qiao, W.M.; Ling, L.C. Preparation of TiO_2/mesoporous carbon composites and their photocatalytic performance for methyl orange degradation. *Xinxing Tan Cailiao/New Carbon Mater.* **2013**, *28*, 47–54. [CrossRef]
40. Shan, R.; Lu, L.; Gu, J.; Zhang, Y.; Yuan, H.; Chen, Y.; Luo, B. Photocatalytic degradation of methyl orange by Ag/TiO_2/biochar composite catalysts in aqueous solutions. *Mater. Sci. Semicond. Process.* **2020**, *114*, 105088. [CrossRef]

Disclaimer/Publisher's Note: The statements, opinions and data contained in all publications are solely those of the individual author(s) and contributor(s) and not of MDPI and/or the editor(s). MDPI and/or the editor(s) disclaim responsibility for any injury to people or property resulting from any ideas, methods, instructions or products referred to in the content.